International Journal of Mass Spectrometry 283 (2009) 105–111

Contents lists available at ScienceDirect

International Journal of Mass Spectrometry

journal homepage: www.elsevier.com/locate/ijms

Aminoglycoside antibiotics: A-site specific binding to 16S

Erin Shammel Baker, Nicholas F. Dupuis, Michael T. Bowers *

Department of Chemistry and Biochemistry, University of California, Santa Barbara, CA 93106-9510, United States

ARTICLE INFO

Article history:
Received 13 January 2009
Received in revised form 9 February 2009
Accepted 11 February 2009
Available online 21 February 2009

Keywords:
Ion mobility
16S
Mass spectrometry

ABSTRACT

The A-site of 16S rRNA, which is a part of the 30S ribosomal subunit involved in prokaryotic translation, is a well known aminoglycoside binding site. Full characterization of the conformational changes undergone at the A-site upon aminoglycoside binding is essential for development of future RNA/drug complexes; however, the massiveness of 16S makes this very difficult. Recently, studies have found that a 27 base RNA construct ($16S_{27}$) that comprises the A-site subdomain of 16S behaves similarly to the whole A-site domain. ESI-MS, ion mobility and molecular dynamics methods were utilized in this study to analyze the A-site of $16S_{27}$ before and after the addition of ribostamycin (R), paromomycin (P) and lividomycin (L). The ESI mass spectrum for $16S_{27}$ alone illustrated both single-stranded $16S_{27}$ and double-stranded $(16S_{27})_2$ complexes. Upon aminoglycoside addition, the mass spectra showed that only one aminoglycoside binds to $16S_{27}$, while either one or two bind to $(16S_{27})_2$. Ion mobility measurements and molecular dynamics calculations were utilized in determining the solvent-free structures of the $16S_{27}$ and $(16S_{27})_2$ complexes. These studies found $16S_{27}$ in a hairpin conformation while $(16S_{27})_2$ existed as a cruciform. Only one aminoglycoside binds to the single A-site of the $16S_{27}$ hairpin and this attachment compresses the hairpin. Since two A-sites exist for the $(16S_{27})_2$ cruciform, either one or two aminoglycosides may bind. The aminoglycosides compress the A-sites causing the cruciform with just one aminoglycoside bound to be larger than the cruciform with two bound. Non-specific binding was not observed in any of the aminoglycoside/$16S_{27}$ complexes.

1. Introduction

RNA is an attractive target for drug discovery due to its well-defined tertiary structure which plays a vital role in cellular functions [1–5]. For several years, RNA/ligand complexes have been analyzed to determine how a bound ligand can effect RNA functionality. One RNA/ligand complex of interest occurs when an aminoglycoside antibiotic binds to prokaryotic 16S rRNA. 16S rRNA is a part of the 30S ribosomal subunit involved in prokaryotic translation and is highly conserved among prokaryotes. Aminoglycosides are known to bind at the A-site domain of 16S (an adenine/2 adenine mismatch in Watson-Crick base pairing), which is normally used by RNA to bind charged aminoacyl tRNA that corresponds to the next mRNA codon in the transcript [6–22]. When the aminoglycoside antibiotics bind to the A-site, they interfere with translation in the ribosome and consequently lead to prokaryotic cell death.

While it is important to understand how the aminoglycosides interact with the whole 16S rRNA region, it is very large and difficult to analyze. However, studies have found that small subdomains can mimic the functional domains of large rRNA strands, and a 27 base RNA construct $rG_2CGUCACAC_2U_2CG_3UGA_2GUCGC_2$ (Scheme 1) has been shown to behave similarly to the A-site domain in the entire 16S rRNA (~1500 bases) [9,19]. The aminoglycoside paromomycin has even been shown to bind to both the A-site domain of 16S and the subdomain of its 27 base construct with similar affinities [13]. For simplicity the 27 base construct of 16S will be referred to as $16S_{27}$ for the rest of the paper.

$16S_{27}$ has allowed the 16S rRNA A-site to be studied extensively by NMR, X-ray crystallography and mass spectrometry [6–22]. NMR structures of $16S_{27}$ before and after paromomycin binds have shown interesting structural variations [7,8]. From the bound NMR structures, it appears that paromomycin binds to two phosphate groups in the major groove of the A-site and displaces the three unpaired adenines towards the minor groove. This alteration causes the paromomycin bound A-site to be more compact than the unbound A-site (Scheme 2), resulting in structural changes. Previously, it has been observed that when aminoglycosides bind to 16S they induce misreading of mRNAs and this conformational change in the A-site may be the origin of this phenomenon [5].

Recently, ESI-MS in combination with ion mobility methods has served to demonstrate that DNA secondary structures such as helices [23–26] and G-quadruplexes [27–31] are stable when

* Corresponding author.
E-mail address: bowers@chem.ucsb.edu (M.T. Bowers).

1387-3806/$ – see front matter © 2009 Elsevier B.V. All rights reserved.
doi:10.1016/j.ijms.2009.02.010

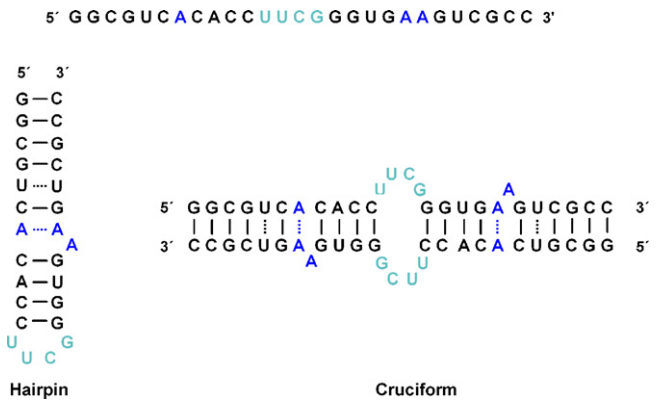

Scheme 1. A schematic of the 27 base construct of the 16S rRNA region ($16S_{27}$). It is possible for this sequence to form a single-stranded hairpin or double-stranded cruciform structure.

sprayed and dehydrated using nano-ESI and they retain most of their solution phase structural characteristics. Knowing that DNA complexes remain intact and retain their solution structure in the gas phase makes ESI-MS in conjunction with ion mobility spectrometry an ideal method for studying the conformational changes that occur in the A-site of $16S_{27}$ upon the binding of the aminoglycosides ribostamycin (R), paromomycin (P) and lividomycin (L) (Scheme 3). R, P and L constitute the 4,5-disubstituted 2-deoxystreptamines class of aminoglycosides and were utilized in this study to understand if binding and induced conformational changes were comparable when aminoglycosides of different sizes were analyzed.

2. Experimental method

2.1. Materials and sample preparation

The 27 base sequence $rG_2CGUCACAC_2U_2CG_3UGA_2GUCGC_2$ ($16S_{27}$) that contained the essential components of the 16S rRNA A-site was obtained from Dharmacon (Boulder, CO). $16S_{27}$ was deprotected according to the manufacturer's directions, ethanol precipitated twice from 1 M ammonium acetate and suspended at a concentration of 1 μM in a 10 mM NH_4OAc/33% IPA/2.86% DMSO solution. The sample was then annealed at 95 °C for 10 min, quickly cooled in an ice bath, and stored at 10 °C. Ribostamycin (R), paromomycin (P) and lividomycin (L) were obtained from Sigma (St. Louis, MO) and used without further purification. They were prepared to a concentration of 1 μM in a 10 mM NH_4OAc/33% IPA/2.86% DMSO solution, added to $16S_{27}$ in various equivalents and incubated at room temperature prior to analysis.

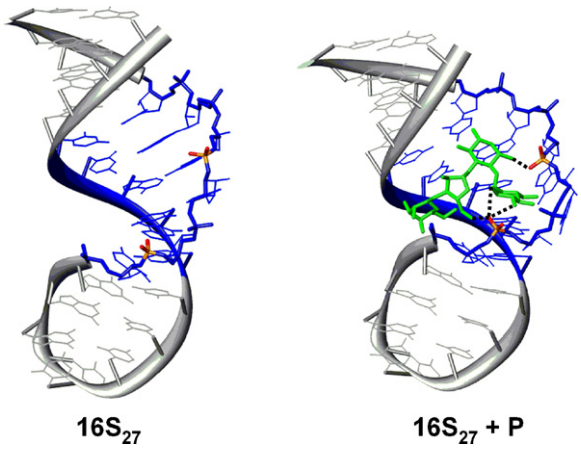

Scheme 2. The NMR structures of $16S_{27}$ alone and $16S_{27}$ with paromomycin (P) bound in its A-site. The binding region is shown in blue, P in green, the two phosphate groups P binds to are highlighted with orange phosphorous atoms and red oxygens. The structure of P is shown in Scheme 3. (For interpretation of the references to colour in this figure legend, the reader is referred to the web version of the article.)

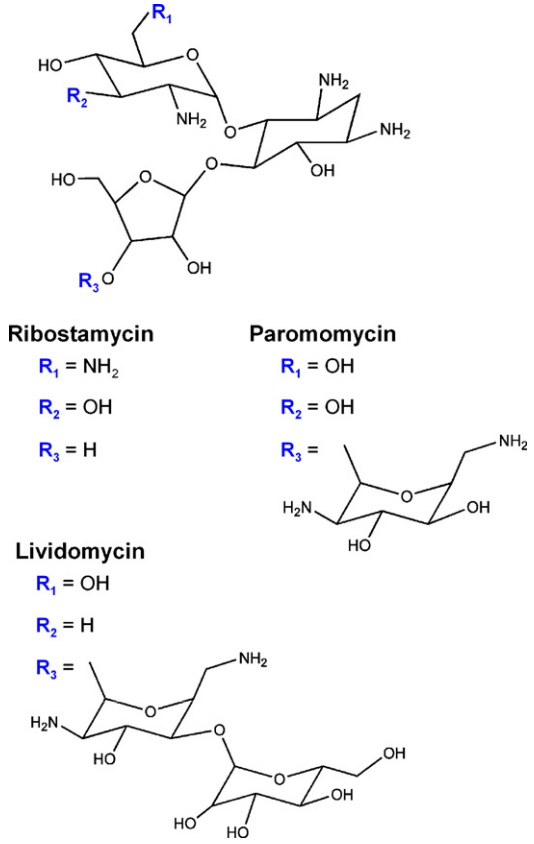

Scheme 3. The three different aminoglycoside antibiotics studied: ribostamycin, paromomycin and lividomycin.

2.2. Mass spectrometry and ion mobility experiments

The details concerning the experimental setup for the mass spectra and ion mobility measurements have been previously published, so only a brief description will be given. Ions were formed by nano-ESI and injected into the specially designed ion funnel of the ESI drift cell instrument [32]. The ions then traveled into a 4.5 cm long drift cell filled with ~5 Torr helium gas and were pulled at a constant drift velocity by a weak, uniform electric field applied across the drift cell. After exiting the drift cell, the ions were mass analyzed in a quadrupole mass filter and detected. The quadrupole mass filter was set to select the mass range of interest for the acquisition of a mass spectrum and in pulsed experiments it was tuned to detect one specific m/z as a function of time, yielding an arrival time distribution or ATD. The reduced mobility, K_o, of the mass-selected ion was obtained from a series of ATDs measured at different electric field strengths (10–23 V/cm) as shown in Eq. (1), where l is the length of the cell, p is the pressure of the He gas (in Torr), V is the electric field voltage, t_A is the ions' arrival time taken from the center of the ATD peak and t_o is the amount of time the ion spends outside the drift cell before reaching the detector.

$$K_o = \left(l^2 \times \frac{273}{760T} \times \frac{p}{V} \times \frac{1}{t_A - t_o}\right) \quad (1)$$

Once K_o is found, the ion's collision cross section, σ, was calculated as shown in Eq. (2)

$$\sigma = \frac{3e}{16N_o}\left(\frac{2\pi}{\mu k_b T}\right)^{1/2}\frac{1}{K_o} \quad (2)$$

where T is the temperature in Kelvin, e is the charge of the ion, N_o is the number density of He at STP, k_b is Boltzmann's constant and μ is the ion-He reduced mass.[33]

2.3. Theoretical calculations

Structural information about the ion mobility experiments was obtained by comparing the experimental cross sections determined from the ATDs to cross sections of theoretical structures. The NMR structures 1A3M [7] and 1J7T [8,34] were utilized in generating the starting structures for $16S_{27}$ and ($16S_{27}$ + P). HyperChem [35] was then used to convert P to R and L for the ($16S_{27}$ + R) and ($16S_{27}$ + L) starting structures. The $(16S_{27})_2$ cruciform structure was fashioned as an A-helix using the NUCGEN utility within AMBER 7 [36], 300 K molecular dynamics simulations were run on each structure for 2 ns using AMBER 7 and every 5 ps a structure was saved. Each structure was then energy minimized and its cross section calculated using hard-sphere scattering and trajectory models developed by the Jarrold group [37,38]. In the calculations, the starting structures eventually converge to give one steady state structure where the cross section remains relatively constant. The average cross sections of the final 50–100 structures in each steady state were used for comparison with the experimental values.

A series of simulated annealing/energy minimization cycles were also used to obtain low-energy globular structures for each complex. In this cycle, the initial structures were energy minimized, annealed at 700 K for 30 ps (to allow the structure to overcome low-lying barriers and change shape), exponentially cooled to 50 K over a variable time step and energy minimized again. The final structure was saved and used as the starting structure for the next annealing/minimization cycle. This process was continued until 300 low-energy structures were generated. The average cross section of the structures with the lowest 5–10 kcal/mol energies was then compared to the experimental values.

3. Results and discussion

3.1. Mass spectra

The nano-ESI mass spectra of $16S_{27}$ alone and with R, P and L are shown in Fig. 1. For $16S_{27}$ with no aminoglycosides added (Fig. 1a), peaks for both $16S_{27}$ and $(16S_{27})_2$ with multiple charge states were observed with NH_4^+ adducts broadening each peak to the high mass side. When the aminoglycosides were added to $16S_{27}$ in a 1 to 1 ratio, peaks for ($16S_{27}$ + X), [$(16S_{27})_2$ + X] and [$(16S_{27})_2$ + 2X], where X = R, P or L, were present in the spectra. However, due to the presence of double-stranded complexes in the mass spectra, care was taken in assigning the single-strand peaks of $16S_{27}^{5-}$ and $(16S_{27} + X)^{5-}$, since they could also correlate with the double-stranded peaks for $(16S_{27})_2^{10-}$ and $[(16S_{27})_2 + 2X]^{10-}$. Thus, to fully characterize the mass spectra, ion mobility measurements were utilized.

3.2. Ion mobility

In order to examine the conformational properties of the $16S_{27}$/aminoglycoside complexes and determine whether the aminoglycosides bind to the A-site of $16S_{27}$, ion mobility experiments were performed.

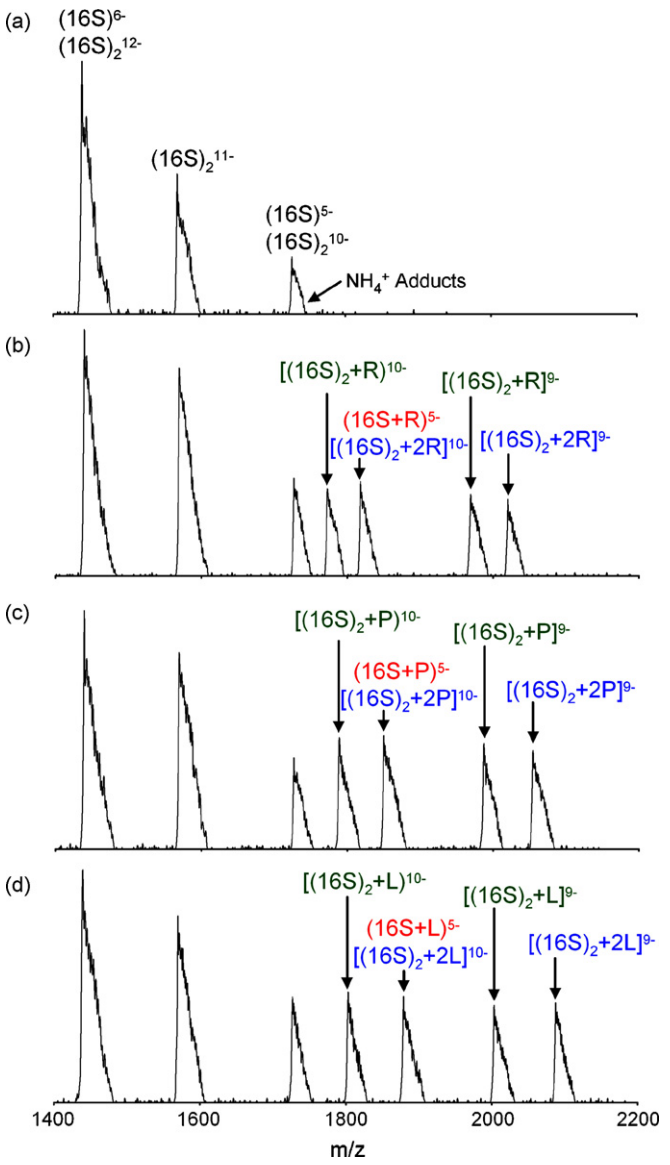

Fig. 1. Nano-ESI mass spectra for (a) $16S_{27}$, (b) $16S_{27}$ with R, (c) $16S_{27}$ with P and (d) $16S_{27}$ with L. NH_4^+ adducts are observed to the right of each peak. All $16S_{27}$ and $(16S_{27})_2$ complexes are labeled in black, ($16S_{27}$ + X) in red, [$(16S_{27})_2$ + X] green and [$(16S_{27})_2$ + 2X] blue, where X = R, P or L. For labeling simplicity, $16S_{27}$ is referred to as 16S in the figure. (For interpretation of the references to colour in this figure legend, the reader is referred to the web version of the article.)

3.3. $16S_{27}$ and $(16S_{27})_2$

The ATDs for $16S_{27}^{5-}$ and $(16S_{27})_2^{11-}$ are shown in Fig. 2. Only one peak was observed in the ATD for $(16S_{27})_2^{11-}$ (Fig. 2b) and this peak can only correspond to a double-stranded structure with a measured cross section of 1675 Å^2 (as the $16S_{27}$ single-strand would need to have a charge state of −5.5). However, two peaks were observed in the $16S_{27}^{5-}$ ATD indicating that either $16S_{27}^{5-}$ has multiple conformers or the $16S_{27}^{5-}$ duplex (i.e. $(16S_{27})_2^{10-}$) occurs in the experiment [25]. It is known that for any given integer charge state, q, observed in a mass spectrum, either a single-strand (S^{q-}) or duplex (D^{2q-}) could exist. Since each of these species has the same m/z value, they are indistinguishable in this mass spectrum. However, for all real systems the cross section of a single-strand is greater than the cross section of a duplex divided by two, resulting in the arrival time of the single-strand being greater than the arrival time of the duplex. This is obvious because the maximum

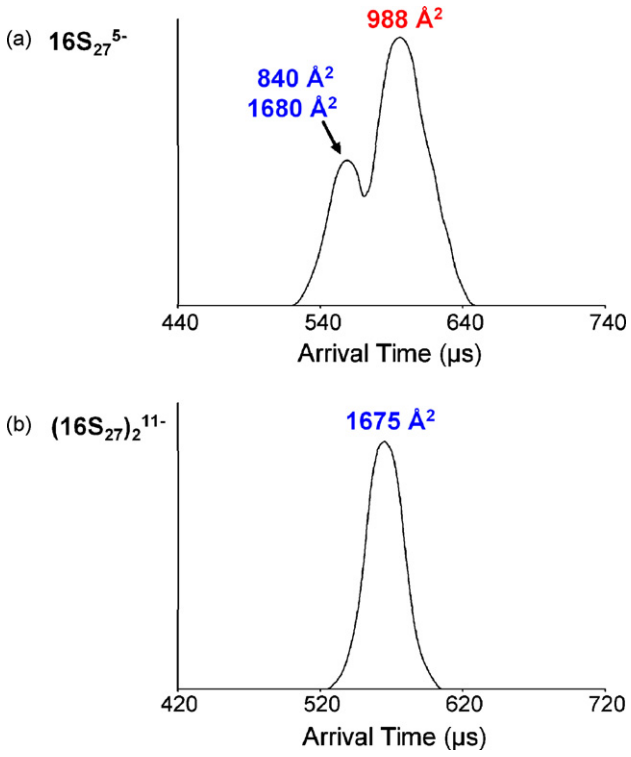

Fig. 2. (a) The ATD for $(16S_{27})_2{}^{10-}$ and $16S_{27}{}^{5-}$. The longer time peak was assigned to $16S_{27}{}^{5-}$, and after theoretical calculations the shorter time peak was determined to be $(16S_{27})_2{}^{10-}$ with a cross section of 1680 Å^2. (b) Only one peak was observed for $(16S_{27})_2{}^{11-}$.

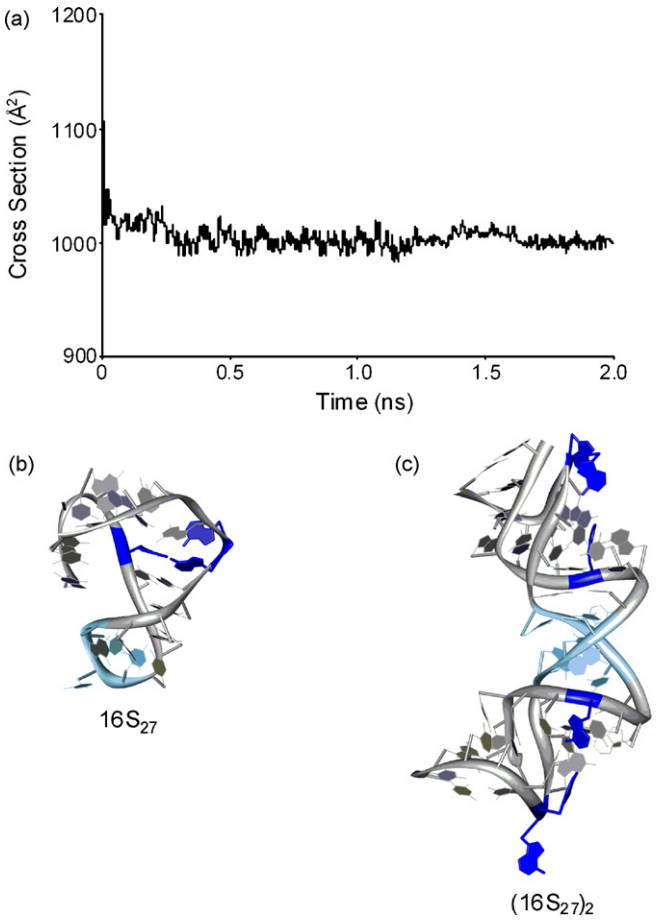

Fig. 3. (a) The plot of cross section versus dynamics time for the $16S_{27}{}^{5-}$ hairpin. Dynamics simulations were run at 300 K for 2 ns and every 5 ps a structure was saved and its cross section calculated. Only one steady state was observed in the dynamics plot for each of the RNA complexes studied. Theoretical structures of (b) $16S_{27}$ and (c) $(16S_{27})_2$ obtained from dynamics calculations. The adenines in the A-sites are shown in dark blue and the tetraloop in $16S_{27}$ and the cruciform mismatch in $(16S_{27})_2$ are shown in light blue (For interpretation of the references to colour in this figure legend, the reader is referred to the web version of the article.).

cross section for a duplex occurs when two single-strand subunits are fully separated and only in this limit does $\sigma(S) = \sigma(D)/2$. As they come closer together, $\sigma(D)/2$ becomes smaller as the two monomers accommodate each other until the final duplex structure transpires. Thus, the peak at shortest time could be due to the double-stranded $(16S_{27})_2{}^{10-}$ instead of $16S_{27}{}^{5-}$. The cross section of each $16S_{27}{}^{5-}$ ATD peak was measured, but since cross section is dependent on charge and mass the longest time peak was calculated as 988 Å^2 for $16S_{27}{}^{5-}$, but the shorter time peak could either be 840 Å^2 for the single-stranded conformation of $16S_{27}{}^{5-}$ or 1680 Å^2 for $(16S_{27})_2{}^{10-}$. Cross sections for both possibilities are given in Fig. 2a.

Theoretical modeling was utilized to determine the identity and conformation of each peak observed in the $16S_{27}{}^{5-}$ ATD. The NMR hairpin conformation of $16S_{27}$ was used as the starting structure for 300 K molecular dynamics simulations [7] and its dynamics plot of cross section versus time is shown in Fig. 3a. Only one steady state at 1000 Å^2 was observed in the dynamics plot and a representative structure is shown in Fig. 3b. Since the cross section for the hairpin only correlates with the longest time ATD peak, globular structures were also calculated (by performing simulated annealing at 700 K on the $16S_{27}$ sequence) to see if they matched the shorter time peak. However, the resulting globular structures had an average cross section of 804 Å^2, which was too small to match the smaller experimental cross section within 2% error.

An A-form $(16S_{27})_2{}^{10-}$ cruciform was used as the starting structure for 300 K dynamics to determine if a double-stranded complex correlated with the shortest time ATD peak. An A-helix was the only form used because it is known that double-stranded RNA is almost always in an A-helix conformation. Only one steady state was observed in the dynamics plot at 1668 Å^2 and a representative structure is shown in Fig. 3c. A globular structure for $(16S_{27})_2{}^{10-}$ with a cross section of 1513 Å^2 was also calculated using simulated annealing. When the experimental cross section for the shortest time peak in the ATD in Fig. 2a was compared to these double-stranded theoretical values, the cruciform matched but the globular structure was too small. This allowed full assignment of the ATD, with the shorter time peak corresponding to the cruciform structure of $(16S_{27})_2{}^{10-}$ and the longer time peak matching the hairpin structure of $16S_{27}{}^{5-}$. The experimental and theoretical cross section values are collected in Table 1.

To understand what happens as the charge states of $16S_{27}$ and $(16S_{27})_2$ become more negative, the cross sections of the other mass spectra peaks were evaluated. Only one peak was observed in the ATD for $(16S_{27})_2{}^{11-}$ (Fig. 2b) and its cross section is very similar to the cross section for the $(16S_{27})_2{}^{10-}$ cruciform (Table 1).

Table 1
Experimental and theoretical cross sections (Å^2) for $16S_{27}$ and $(16S_{27})_2$.

Complex	Expt[a]	Theory[b]		
		Hairpin	Cruciform	Globular
$16S_{27}{}^{5-}$	988	1000	–	804
$16S_{27}{}^{6-}$	1008	1016	–	806
$(16S_{27})_2{}^{10-}$	1680	–	1668	1513
$(16S_{27})_2{}^{11-}$	1675	–	1674	1512
$(16S_{27})_2{}^{12-}$	1694	–	1683	1515

[a] 1% reproducibility error.
[b] ≤2% standard deviation.

The ATD for the $16S_{27}{}^{6-}/(16S_{27})_2{}^{12-}$ had two peaks similar to the $16S_{27}{}^{5-}/(16S_{27})_2{}^{10-}$ ATD and when theoretical modeling was performed, the shorter time peak correlated with the cruciform of $(16S_{27})_2{}^{12-}$ and the longer time peak matched the $16S_{27}{}^{6-}$ hairpin (Table 1). In all cases, the calculated cross sections were within 1% of the experimental values allowing the unambiguous assignment of the conformation of $16S_{27}$ to a hairpin and $(16S_{27})_2$ to a cruciform. Strand fraying and elongation with charge state which has previously been observed in the gas phase with smaller hairpin structures, was not observed with the $16S_{27}$ hairpin due to its increased number of stabilizing hydrogen bonds [26].

3.4. $16S_{27}$ and $(16S_{27})_2$ with R, P and L

A typical ATD for the $(16S_{27}+X)^{5-}$ complexes, where X = R, P or L, is shown in Fig. 4a. Two peaks were present in the ATDs for all three aminoglycosides and similar to $16S_{27}{}^{5-}$ without any aminoglycosides bound, the longer time peak corresponds to $(16S_{27}+X)^{5-}$ and the shorter time peak probably correlates to $[(16S_{27})_2+2X]^{10-}$. To further analyze the shorter time peak and eliminate any contributions from the $(16S_{27}+X)$ complexes, the −9 charge state of $[(16S_{27})_2+2X]$ was evaluated. For all three aminoglycosides, the $[(16S_{27})_2+2X]^{9-}$ complex only had one conformation (Fig. 4b) and its experimental cross section agreed within 1% of the cross section values for the shorter time peak in Fig. 4a indicating that $[(16S_{27})_2+2X]^{10-}$ probably correlates with this peak. When the $[(16S_{27})_2+X]^{9-}$ complexes with only one aminoglycoside bound were analyzed, again only one peak was observed in the ATDs for all

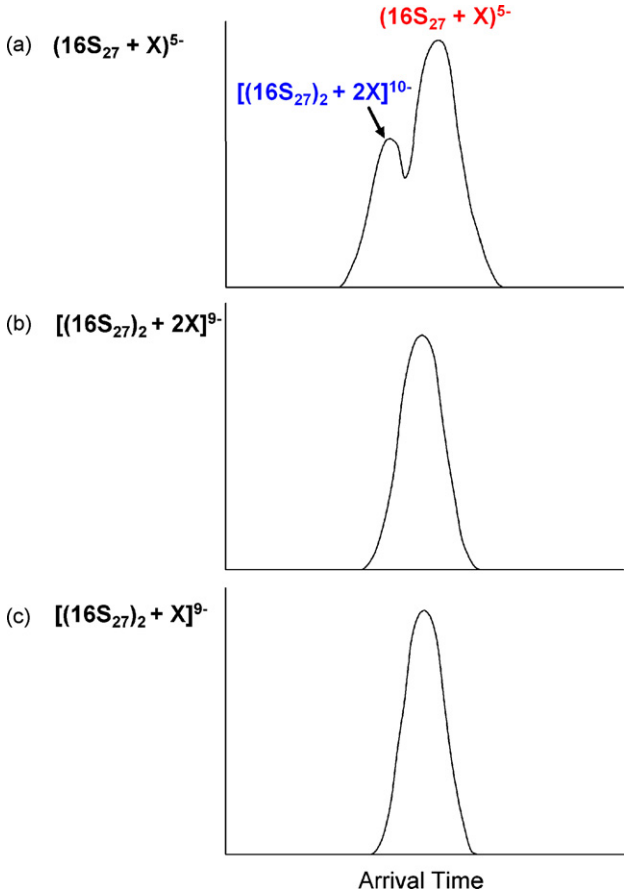

Fig. 4. (a) A typical ATD for $(16S_{27}+X)^{5-}$, where X = R, P or L. The two peaks are assigned to $[(16S_{27})_2+2X]^{10-}$ and $(16S_{27}+X)^{5-}$. (b) $[(16S_{27})_2+2X]^{9-}$ and (c) $[(16S_{27})_2+X]^{9-}$ only had one peak in their ATDs. All of the ATDs shown are for $16S_{27}$ with P, but similar peak ratios were observed for the $(16S_{27}+X)^{5-}$ complexes with R and L.

Table 2
Experimental and theoretical cross sections (Å^2) of the $16S_{27}$ and $(16S_{27})_2$ aminoglycoside antibiotic complexes.

Complex	Expt[a]	Theory[b]	
		Antibiotic bound to A-site	Antibiotic bound non-specifically
$(16S_{27}+R)^{5-}$	910	919	999
$(16S_{27}+P)^{5-}$	909	918	1007
$(16S_{27}+L)^{5-}$	907	915	1004
$[(16S_{27})_2+R]^{9-}$	1595	1600	1675
$[(16S_{27})_2+P]^{9-}$	1606	1604	1678
$[(16S_{27})_2+L]^{9-}$	1603	1609	1669
$[(16S_{27})_2+2R]^{9-}$	1541	1550	1683
$[(16S_{27})_2+2P]^{9-}$	1550	1548	1690
$[(16S_{27})_2+2L]^{9-}$	1552	1543	1686

[a] 1% reproducibility error.
[b] ≤2% standard deviation.

three aminoglycosides (Fig. 4c). All the cross sectional values corresponding to $(16S_{27}+X)^{5-}$, $[(16S_{27})_2+X]^{9-}$ and $[(16S_{27})_2+2X]^{9-}$ are listed in Table 2. The values for $[(16S_{27})_2+2X]^{10-}$ were within 1% of $[(16S_{27})_2+2X]^{9-}$, so they are not illustrated in the table.

The experimental cross sections for the $(16S_{27}+X)^{5-}$ complexes are all very similar suggesting that R, P and L bind to the same area of $16S_{27}$. In order to determine possible structures for $(16S_{27}+X)^{5-}$, 300 K molecular dynamics calculations were performed on complexes with the aminoglycosides bound in the A-site of the hairpin as shown in Fig. 5a. Non-specific binding was also evaluated with the aminoglycosides bound at random sites on $16S_{27}$. One steady state was observed in all of the dynamics plots similar to Fig. 3a, however, different cross sections were observed for the aminoglycosides bound in the A-site versus non-specifically bound. Only the theoretical cross sections for the A-site bound aminoglycosides agreed with the experimental data (Table 2), while all of the non-specifically bound complexes were too large, indicating that the aminoglycosides R, P and L only bind in the A-site. Representative solvent-free structures of $(16S_{27}+X)^{5-}$ are shown in Fig. 5b. When the starting NMR structure is compared with its corresponding solvent-free structure, it appears that the solvent-free structures are more compact that the solution structures. It was also observed that the solvent-free aminoglycoside complexes retain the helical turn of $16S_{27}$, while $16S_{27}$ without any aminoglycosides starts to unfold (Fig. 5b).

When the cross sections of the three $[(16S_{27})_2+X]^{9-}$ complexes with R, P and L were compared, they all had very similar values. This was also true for the three $[(16S_{27})_2+2X]^{9-}$ complexes, indicating that all three aminoglycosides must effect $(16S_{27})_2$ in very similar ways. However, when the $(16S_{27})_2$ complexes with one aminoglycoside were compared to the complexes with two, the cross sections for the $[(16S_{27})_2+X]^{9-}$ complexes were larger implying that the addition of one extra aminoglycoside increases the compactness of $(16S_{27})_2$. The structures of the $(16S_{27})_2$ cruciform with one and two aminoglycosides were evaluated to determine the binding site(s). Since $(16S_{27})_2$ has two A-sites, it seems reasonable that the aminoglycosides might bind to one or both. $(16S_{27})_2$ complexes with more than 2 aminoglycosides bound were not observed, suggesting that non-specific binding does not take place. 300 K molecular dynamics were performed on the cruciforms with the aminoglycosides both in the A-site and non-specifically bound. Only one steady state was observed for each structure and the cross sections are given in Table 2. The only theoretical cross sections that correlated with the experimental values had the aminoglycosides bound in the A-site, similar to the single-stranded structures. Representative theoretical structures for $[(16S_{27})_2+X]^{9-}$ and $[(16S_{27})_2+2X]^{9-}$ are shown in Fig. 6.

Conformational changes were observed in the theoretical structures when the aminoglycosides bind to $(16S_{27})_2$. The theoretical

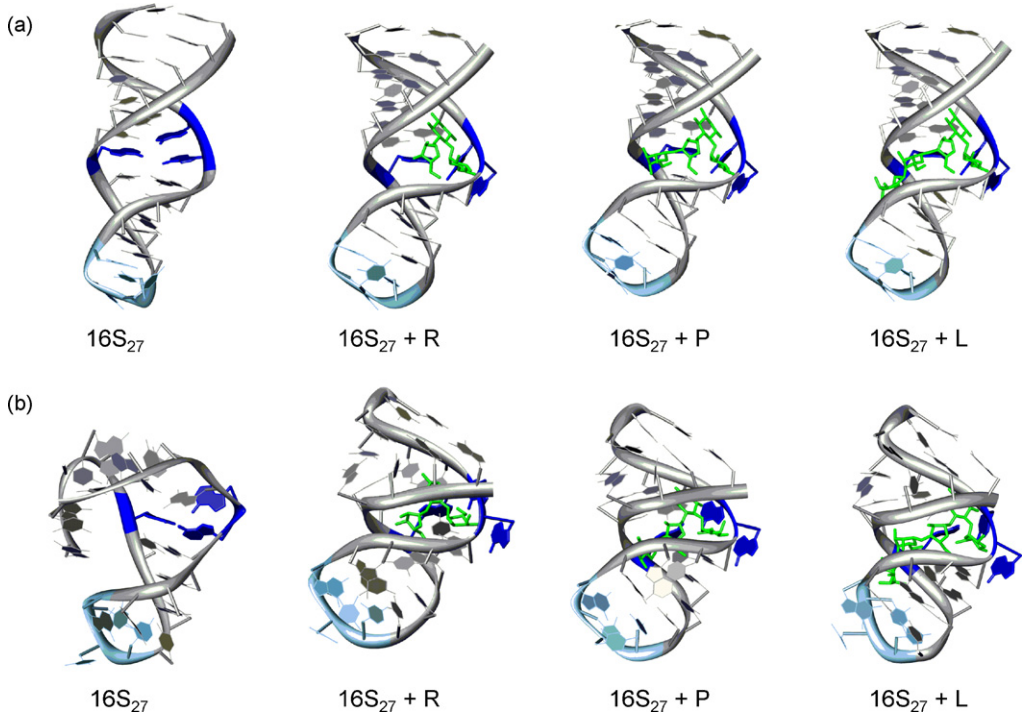

Fig. 5. (a) The starting structures for each hairpin complex derived from the NMR structures for $16S_{27}$ and ($16S_{27}$ + P). (b) The resulting solvent-free theoretical structures for each $16S_{27}$ complex obtained from MD simulations. The adenines in the A-site are shown in dark blue, the tetraloop is light blue and each aminoglycoside is green. (For interpretation of the references to colour in this figure legend, the reader is referred to the web version of the article.)

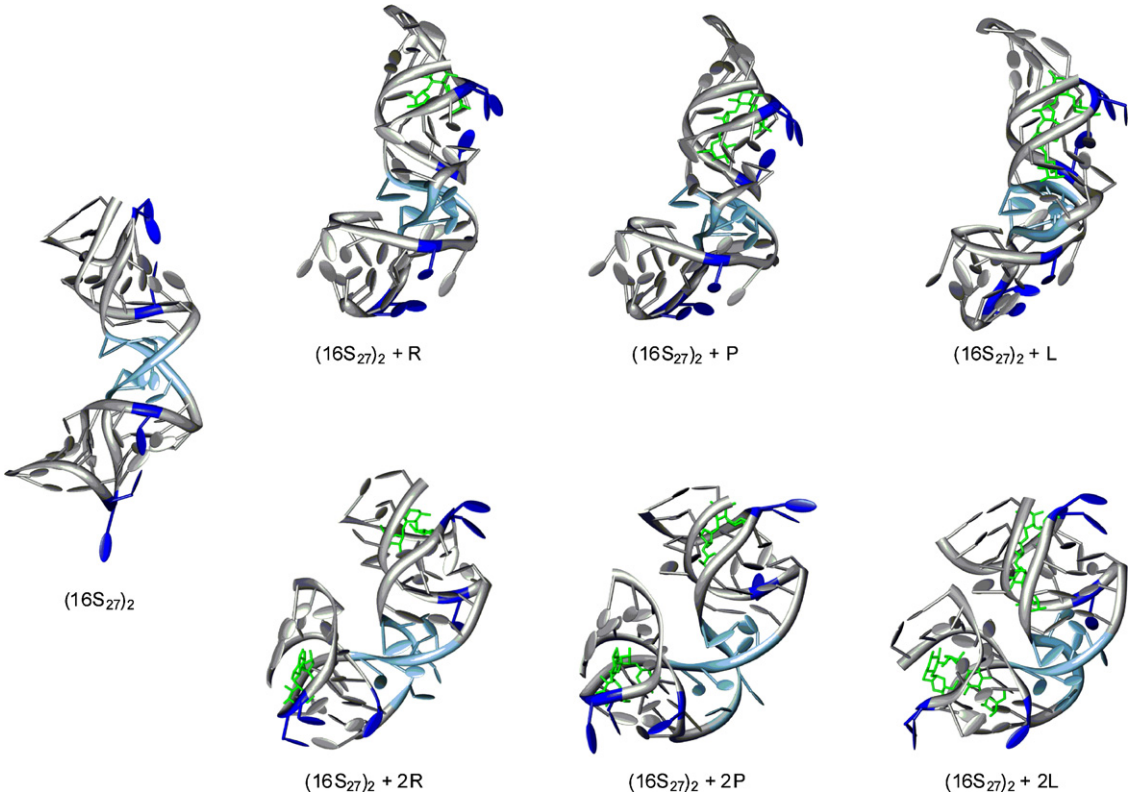

Fig. 6. The theoretical structures for $(16S_{27})_2$ and the $(16S_{27})_2$ complexes with 1 and 2 antibiotics. The adenines in the A-site are shown in dark blue, the four base mismatch is light blue, each antibiotic is green and the bases are shown as slabs for clarity. (For interpretation of the references to colour in this figure legend, the reader is referred to the web version of the article.)

structure of $(16S_{27})_2$ is larger than $(16S_{27})_2$ with one aminoglycoside bound in the A-site (Fig. 6). And when two aminoglycosides bind to $(16S_{27})_2$, a further compaction of the cruciform is observed. This trend indicates that, similar to the NMR structures shown in Scheme 2, the aminoglycosides compress the A-site. The compression of the A-site affects the structure of $16S_{27}$ and this structural alteration possibly interferes with the ability of 16S to perform translation in the ribosome.

4. Summary

The mass spectrometry, ion mobility, and molecular dynamics results presented provide insight into the binding of aminoglycoside antibiotics to $16S_{27}$. In particular, we conclude:

(1) Both $16S_{27}$ and $(16S_{27})_2$ are present in the mass spectrum of the $16S_{27}$ solution. Ion mobility calculations indicate that $16S_{27}$ is in a hairpin conformation, while $(16S_{27})_2$ is a double-stranded cruciform.
(2) Ribostamycin, paromomycin and lividomycin all bind to $16S_{27}$ and $(16S_{27})_2$, but only one aminoglycoside binds to $16S_{27}$, while either one or two aminoglycosides binds to $(16S_{27})_2$.
(3) Ion mobility measurements and molecular dynamics calculations indicate that the aminoglycosides bind in the single A-site of $16S_{27}$ and the two A-sites of $(16S_{27})_2$. Non-specific binding does not occur in any of the complexes.
(4) The cross sections for $16S_{27}$ and $(16S_{27})_2$ decrease upon aminoglycoside binding indicating that the aminoglycosides compress the A-site and in turn alter the structure of each RNA complex.

Acknowledgements

The support of the National Science Foundation under grant CHE-0503728 is gratefully acknowledged. Also, assistance with the sample preparation from Dr. Kristin Saunds-Lowery and Dr. Steven A. Hofstadler at Ibis Therapeutics is greatly appreciated.

References

[1] T. Herman, E. Westhof, Combinatorial Chem. 3 (2000) 219.
[2] S.J. Sucheck, C.-H. Wong, Curr. Opin. Chem. Biol. 4 (2000) 678.
[3] A. Ramos, C.C. Gubser, G. Varani, Curr. Opin. Struct. Biol. 7 (1997) 317.
[4] G.L. Conn, D.E. Draper, Curr. Opin. Struct. Biol. 8 (1998) 278.
[5] R.T. Batey, R.P. Rambo, J.A. Doudna, Angew. Chem. Int. Ed. 38 (1999) 2326.
[6] D. Moazed, H.F. Noller, Nature 327 (1987) 389.
[7] D. Fourmy, S. Yoshizawa, J.D. Puglisi, J. Mol. Biol. 277 (1998) 333.
[8] Q. Vicens, E. Westhof, J. Mol. Biol. 326 (2003) 1175.
[9] D. Fourmy, M.I. Recht, S.C. Blanchard, J.D. Puglisi, Science 274 (1996) 1367.
[10] M.I. Recht, D. Fourmy, S.C. Blanchard, K.D. Dahlquist, J.D. Puglisis, J. Mol. Biol. 262 (1996) 421.
[11] Y. Wang, K. Hamasaki, R.R. Rando, Biochemistry 36 (1997) 768.
[12] D. Fourmy, M.I. Recht, J.D. Puglisi, J. Mol. Biol. 277 (1998) 347.
[13] C.-H Wong, M. Hendrix, E.S. Priestley, W.A. Greenberg, Chem. Biol. 5 (1998) 397.
[14] M.I. Recht, S. Douthwaite, K.D. Dahlquist, J.D. Puglisi, J. Mol. Biol. 286 (1999) 33.
[15] A.P. Carter, W.M. Clemons, D.E. Brodersen, R.J. Morgan-Warren, B.T. Wimberly, V. Ramakrishnan, Nature 407 (2000) 340.
[16] B.T. Wimberly, D.E. Brodersen, W.M. Clemons, R.J. Morgan-Warren, A.P. Cater, C. Vonrhein, T. Hartsch, V. Ramakrishnan, Nature 407 (2000) 327.
[17] D.H. Ryu, R.R. Rando, Bioorg. Med. Chem. 9 (2001) 2601.
[18] S.R. Lynch, J.D. Puglisi, J. Mol. Biol. 306 (2001) 1037.
[19] P. Purohit, S. Stern, Nature 370 (1994) 659.
[20] K.A. Sannes-Lowery, R.H. Griffey, S.A. Hofstadler, Anal. Biochem. 280 (2000) 264.
[21] R.H. Griffey, S.A. Hofstadler, K.A. Sannes-Lowery, D.J. Ecker, S.T. Crooke, Proc. Natl. Acad. Sci. U.S.A. 96 (1999) 10129.
[22] J.M. Ogle, D.E. Brodersen, W.M. Clemons Jr., M.J. Tarry, A.P. Carter, V. Ramakrishnan, Science 292 (2001) 897.
[23] J. Gidden, A. Ferzoco, E.S. Baker, M.T. Bowers, J. Am. Chem. Soc. 126 (2004) 15132.
[24] J. Gidden, E.S. Baker, A. Ferzoco, M.T. Bowers, Int. J. Mass Spectrom. 240 (2005) 183.
[25] E.S. Baker, M.T. Bowers, J. Am. Soc. Mass Spectrom. 18 (2007) 1188.
[26] E.S. Baker, N.F. Dupuis, M.T. Bowers, J. Phys. Chem. B 113 (2009) 1722.
[27] E.S. Baker, S.L. Bernstein, M.T. Bowers, J. Am. Soc. Mass Spectrom. 16 (2005) 989.
[28] E.S. Baker, S.L. Bernstein, V. Gabelica, E. De Pauw, M.T. Bowers, Int. J. Mass Spectrom. 253 (2006) 225.
[29] V. Gabelica, E.S. Baker, M.-P. Teulande-Fichou, E. De Pauw, M.T. Bowers, J. Am. Chem. Soc. 129 (2007) 895.
[30] E.S. Baker, J.T. Lee, J.L. Sessler, M.T. Bowers, J. Am. Chem. Soc. 128 (2006) 2641.
[31] N. Smargiasso, F. Rosu, W. Hsia, P. Colson, E.S. Baker, M.T. Bowers, E. De Pauw, V. Gabelica, J. Am. Chem. Soc. 130 (2008) 10208.
[32] T. Wyttenbach, P.R. Kemper, M.T. Bowers, Int. J. Mass Spectrom. 212 (2001) 13.
[33] E.A. Mason, E.W. McDaniel, Transport Properties of Ions in Gases, Wiley, New York, NY, 1988.
[34] H.M. Berman, J. Westbrook, Z. Feng, G. Gilliland, T.N. Bhat, H. Weissig, I.N. Shindyalov, P.E. Bourne, The Protein Data Bank, Nucleic Acids Research 28 (2000) 235.
[35] HyperChem 7.0, Hypercube Inc., 2002.
[36] D.A. Case, D.A. Pearlman, J.W. Caldwell, T.E. Cheatham III, J. Wang, W.S. Ross, C.L. Simmerling, T.A. Darden, K.M. Merz, R.V. Stanton, A.L. Cheng, J.J. Vincent, M. Crowley, V. Tsui, H. Gohlke, R.J. Radmer, Y. Duan, J. Pitera, I. Massova, G.L. Seibel, U.C. Singh, P.K. Weiner, P.A. Kollman, AMBER, vol. 7, University of California, San Francisco, 2002.
[37] M.F. Mesleh, J.M. Hunter, A.A. Shvartsburg, G.C. Schwartz, M.F. Jarrold, J. Phys. Chem. 100 (1996) 16082.
[38] A.A. Shvartsburg, M.F. Jarrold, Chem. Phys. Lett. 261 (1996) 86.